Coupled-mode description for the polarization state of a vertical-cavity semiconductor laser

A. K. Jansen van Doorn, M. P. van Exter, A. M. van der Lee, and J. P. Woerdman

Huygens Laboratory, Leiden University, P.O. Box 9504, 2300 RA Leiden, The Netherlands

For symmetry reasons, vertical-cavity semiconductor lasers might be expected to show polarization isotropy. Practical devices, however, operate in a well-defined polarization state, which indicates the presence of residual anisotropies. We have performed a systematic experimental study of these residual anisotropies by applying additional anisotropies in a controlled and continuous way. The results are compared with a coupled-mode model that describes the effect of linear anisotropies on the polarization eigenmodes. We conclude that the polarization state of a practical device is dominantly determined by these linear anisotropies; nonlinear anisotropies are found to play at most a minor role. [S1050-2947(97)05202-5]

I. INTRODUCTION

During the last decade, a major effort has been put into development of vertical-cavity surface-emitting lasers (VCSELs). This novel type of semiconductor laser has some distinct advantages compared to conventional edge-emitting semiconductor lasers. Most of these advantages are related to the fact that the light is emitted in the vertical direction, i.e., normal to the semiconductor wafer. This feature opens the possibility to fabricate two-dimensional arrays of lasers, allows for on-wafer testing of the devices, and gives a large freedom for shaping the transverse waveguide.

Cylindrical symmetry of the transverse optical confinement, which is advantageous for, e.g., coupling into fibers, is naturally achieved in a VCSEL. This has interesting consequences for their polarization properties: contrary to the situation for edge-emitting semiconductor lasers, where the stripe waveguide has a strong anisotropy, the transverse symmetry of the waveguide of a VCSEL imposes in principle no constraints on the polarization. Also the commonly used cubic crystalline materials, in our case $Al_xGa_{1-x}As$, are optically isotropic, at least as far as their linear optical properties are concerned. For completeness we note that this isotropy is generally broken by the use of quantum wells as active medium [1–3]. For VCSELs grown on the usual (100) substrate, however, the linear optical properties are again isotropic for light propagating normal to the substrate [1,2].

Practical VCSELs are reported to emit linearly polarized light. The orientational stability of this polarization, however, is poor: the orientation shows a rather large spread for different VCSELs of the same array, generally with a preference for the [110] or [1$\bar{1}$0] crystalline axes [4–11]. It has been found that considerable changes of this orientation may occur upon changing either the injection current or the operating temperature [4–6]. Also bistability of two linear polarizations (polarization switching) is often reported [6–10]. That in fact there is a preference for a particular polarization indicates the presence of residual optical anisotropies. A frequently reported example of such an anisotropy is birefringence, which may result from residual strain left during the fabrication process [6,7,11].

For applications, the poor orientational stability of the polarization is a disadvantage. Therefore several methods have

been proposed and demonstrated to stabilize the polarization properties. These methods aim at the introduction of structural anisotropy to invoke a specific polarization preference [1–3,12–17]. Although it has been shown that the polarization can thus be manipulated, the stabilization achieved is never complete. A possible explanation for this limited success is that the intentionally introduced anisotropies are not sufficiently large to dominate unintentional ones. Clearly, successful stabilization of the polarization requires knowledge of the relative importance of the various anisotropies.

In this article we present a systematic experimental and theoretical study of the combined effect of various optical anisotropies that are possible in a VCSEL. The experimental approach we follow is to add a controlled amount of anisotropy and study its effect on the polarization state. Experimentally, we use two controlled anisotropies, namely, strain-induced linear birefringence produced with the so-called hot-spot technique [18,19], and circular birefringence produced by the application of a magnetic field [20]. The aim of our study is threefold: (i) we develop a unified theoretical framework for describing the combined effect of all conceivable linear anisotropies on the polarization behavior, (ii) we experimentally confirm some of the key predictions of this linear model, and (iii) we explore the validity regime of this linear model by realizing situations where the dominant native anisotropy, namely, birefringence, has been canceled almost perfectly by applying a controlled additional birefringence with opposite polarity. For sufficiently good cancellation one would expect the nonlinear anisotropy associated with gain saturation to take over.

The outline of the article is as follows. In Sec. II we present a linear mode-coupling model for the intracavity field to describe the influence of various optical anisotropies on the stationary polarization states. The VCSELs and the experimental techniques are described in Sec. III. In Sec. IV we concentrate on situations in which birefringence is the dominant native anisotropy in the devices; the effect of addition of linear and circular birefringence is discussed in terms of the mode-coupling model and experimentally demonstrated. In Sec. V we explore situations in which birefringence no longer dominates the polarization state, by aiming at complete cancellation of the native birefringence. We end in Sec. VI with a concluding discussion.

II. THEORETICAL FRAMEWORK

Generally, the polarization state of a laser depends on anisotropies of the passive cavity and of the gain medium. To describe the effect of these anisotropies we write the electric field in the cavity by $\vec{E}(t)\exp(i\omega_0 t)$, where $\vec{E}(t)$ denotes the vectorial amplitude and ω_0 the angular frequency of the emitted light. The vectorial amplitude $\vec{E}(t)$ then satisfies the following differential equation [21–23]:

$$i\,\frac{\partial \vec{E}}{\partial t} = -\widetilde{A}\vec{E} + \widetilde{S}\vec{E} - (\cdots \vec{E}\vec{E}\vec{E}\cdots), \qquad (1)$$

where $\widetilde{A}$ is a tensor that describes the properties of the empty cavity (loss and dispersion) and $\widetilde{S}$ is a tensor that describes the linear (i.e., unsaturated) gain and its associated dispersion. The last term in the equation symbolically indicates the saturation of the gain (and its associated dispersion) by stimulated emission. To obtain this equation, both the inversion and the dipole moment have been adiabatically eliminated; therefore we may use Eq. (1) to describe polarization behavior on a time scale which is long as compared to the lifetime of the inversion and the dipole moment.

The polarization eigenmodes and eigenfrequencies of the laser are determined by the anisotropic part of the right-hand side of Eq. (1). This problem has been extensively studied for gas lasers, both experimentally and theoretically [21–23]. In that case the linear gain tensor is a scalar and the polarization is determined by the anisotropy of the empty cavity (i.e., the tensor $\widetilde{A}$) and that of the gain saturation. The latter anisotropy is associated with the anisotropy of the electronic wave functions of the excited-state and ground-state atoms that constitute the gain medium. The eventual polarization state will be the result of a subtle interplay of the saturation effects with the linear anisotropies in the system.

As demonstrated in this article, restriction to the linear terms in Eq. (1) is in most cases sufficient to describe the polarization behavior of practical VCSELs. In fact, in order to distinguish linear from nonlinear effects, a thorough understanding of the linear problem is a prerequisite anyway. We start therefore by considering the linear part of Eq. (1), which can be written as

$$\frac{\partial \vec{E}}{\partial t} = i\widetilde{M}\vec{E}, \qquad (2)$$

where we have combined the matrix for the gain and that for the cavity to $\widetilde{M} \equiv \widetilde{A} - \widetilde{S}$. The stable polarization states are found by solving the eigenstates of $\widetilde{M}$ in Eq. (2). The eigenvalues correspond to the complex eigenfrequencies of the polarization eigenmodes. The real part corresponds to a (real) frequency, and the imaginary part to a damping. The eigenvectors describe the polarization states of the eigenmodes, which will generally be elliptically polarized.

The four tensor components $M_{i,j}$ are generally complex, so that in total eight real parameters are needed to describe $\widetilde{M}$. If we transform the isotropic part, i.e., the average frequency and damping of the two modes, away from Eq. (2), we are left with six real parameters. The resulting traceless tensor can always be separated in a Hermitian and an anti-Hermitian part, i.e.,

$$\widetilde{M} = \tfrac{1}{2}(\widetilde{M} + \widetilde{M}^\dagger) + \tfrac{1}{2}(\widetilde{M} - \widetilde{M}^\dagger), \qquad (3)$$

where $\widetilde{M}^\dagger$ denotes the Hermitian conjugate of $\widetilde{M}$. The Hermitian part describes phase anisotropies. For comparison with experiment, we distinguish between linear and circular birefringence, leading to detuning of, respectively, linearly and circularly polarized states. The anti-Hermitian part describes amplitude anisotropies. Again we distinguish between linear and circular dichroism. In total four parameters are needed to describe the magnitudes of all these optical anisotropies, whereas two more are needed to describe the orientations of the linear birefringence and the linear dichroism, respectively [21]. The identification of the six independent parameters with the optical cavity anisotropies is only valid when the change of the polarization state per cavity round-trip is small [21], as is generally the case for a VCSEL. When we choose a basis along the axes of one of the linear anisotropies, which may always be done, only the relative orientation between the linear birefringence and the linear dichroism enters the problem; we are then left with five instead of six parameters. It can be shown that the occurrence of circular birefringence and circular dichroism requires the presence of a magnetic field [24]. Thus, except for Sec. IV B where we discuss the effect of a magnetic field, we only need to consider linear birefringence and linear dichroism.

It is interesting to note that Eq. (2) represents the general two-mode coupling problem which has realizations in many subfields of physics [25]. In terms of the general coupling formalism, the diagonal elements describe the (complex) detuning of the basis states, whereas the off-diagonal elements describe their coupling. In our case, we apply either linear or circular birefringence to the devices, and we study the frequency splitting and the polarization state of the VCSEL eigenmodes as a function of the strength of the applied anisotropy. Application of linear and circular birefringence corresponds to a (real) detuning of a linearly or circularly polarized basis set, respectively, and the behavior of the frequency splitting and the polarization state will depend on the coupling between these basis states introduced by the native anisotropies in the VCSEL. As generally all native anisotropies need to be considered, the behavior of the mode splitting and polarization state as a function of the applied anisotropy can be rather complicated. It is therefore instructive to consider first the special case that the coupling matrix $\widetilde{M}$ in Eq. (2) is given by:

$$\widetilde{M} = \begin{pmatrix} \delta & M_{12} \\ M_{21} & -\delta \end{pmatrix}. \qquad (4)$$

In this expression, δ denotes the strength of the controlled anisotropy and the native anisotropies enter only as the off-diagonal elements M_{12} and M_{21}, i.e., they lead to a "pure" coupling. The case where the coupling in Eq. (4) is Hermitian ($M_{12} = M_{21}^*$) represents so-called conservative coupling [25]. The eigenvalues of Eq. (2) are always real, with frequencies ω given by

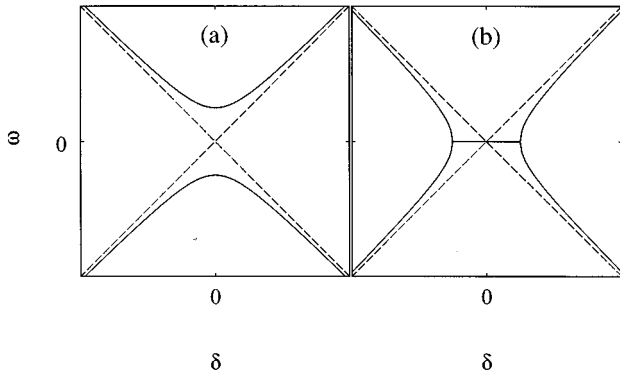$$\omega_\pm = \pm \sqrt{\delta^2 + |M_{12}|^2}. \qquad (5)$$

FIG. 1. Eigenfrequencies ω as a function of detuning δ for (a) conservative and (b) dissipative coupling. The dashed lines represent the eigenfrequencies without coupling ($M_{12}=M_{21}=0$).

This avoided crossing behavior of the eigenfrequencies as a function of the detuning δ is depicted by the solid curves in Fig. 1(a). As compared to the uncoupled case ($M_{12}=M_{21}=0$, indicated with the dashed lines in the figure), the eigenfrequencies of the coupled eigenmodes are pushed apart by the coupling.

The case where the coupling in Eq. (4) is anti-Hermitian ($M_{12}=-M_{21}^{*}$) represents so-called dissipative coupling [25]. The eigenfrequencies are now given by

$$\omega_{\pm}=\pm\sqrt{\delta^2-|M_{12}|^2}. \qquad (6)$$

As shown in Fig. 1(b), the eigenfrequencies are now pulled together by the coupling as compared to the situation without coupling (dashed lines). They become imaginary for $|\delta|<|M_{12}|$, which means that the eigenmodes have the same frequency (''frequency locking'') but a different damping.

III. EXPERIMENTAL TECHNIQUES

In the experiments we use electrically pumped planar VCSELs, grown on (100) substrates [26]. The devices have 1λ cavities with three GaAs quantum wells, are proton implanted for current confinement, and operate at 850 nm. The experiments are restricted to the range of injection currents where only the fundamental transverse TEM$_{00}$ mode is present. For all devices we studied, this single-mode operation extends to at least 1.6 times the threshold current I_{thr}, with $I_{\mathrm{thr}}\approx5$ mA. High-resolution spectral measurements reveal that two polarization modes are present. Figure 2 gives an example of a spectrum, measured with a planar Fabry-Pérot interferometer. The solid curve represents a polarization-unresolved measurement, showing only the narrow lasing component. The dotted curve is a measurement for which the lasing polarization component has been maximally blocked with a crossed Glan-Thomson polarizer. This reveals a broader and much weaker component at the low-frequency side of the lasing component, which is fed by spontaneous emission. The polarization of this component is orthogonal to that of the lasing mode. The two components are spectrally nondegenerate as a result of residual birefringence in the devices. For the devices we studied the magnitude of the native spectral splitting $\Delta\omega_0/2\pi$ varied between 0 and 30 GHz; the spread in $\Delta\omega_0$ is ascribed to random strain
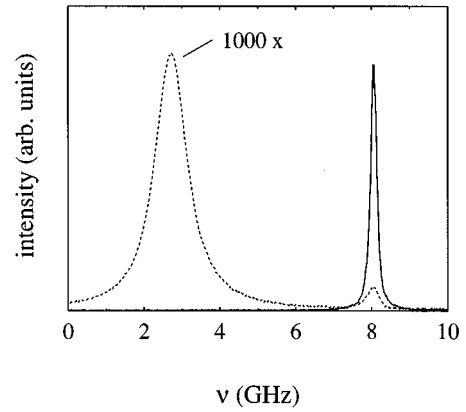

FIG. 2. Typical Fabry-Pérot spectrum of VCSEL, measured without polarizer (solid curve) and with polarizer set for maximum blocking of the lasing component (dotted curve), which reveals also the orthogonally polarized spontaneous emission component.

[18,19]. As a result of this random strain, the native polarization orientation ϕ_0 also varies from device to device; the distribution of polarization angles is not isotropic, but is peaked around the face-diagonal crystalline axis [110] or [1$\bar{1}$0]. This tendency to align with the face-diagonal crystal axes has been shown to result from a pronounced anisotropy in the relation between strain and birefringence [19].

For most of our experiments, devices are used in which the native strain has been changed in a permanent way with a localized damage technique [27]. This technique consists of locally melting the surface of the wafer by focusing a powerful laser beam next to the electrical bond pad of the VCSEL. The stress profile around the damage spot leads to a change of the strain in the aperture of the VCSEL, and thus to an irreversible change of the native birefringence in the VCSEL. By choosing the proper position of the damage spot, the birefringence can, within certain limits, be changed at will. The technique generally does not affect the overall output characteristics of the devices, which can be understood by considering that the strain induced in the aperture of the VCSEL is relatively small [19,27]. The technique allows us to prepare devices with arbitrary birefringence splitting and polarization orientation, so that we do not have to depend on the statistical distribution of these parameters over an array to select a ''suitable'' device for a specific experiment. In the following, the word ''native'' is also meant to include such suitably prepared devices.

For accurate determination of the polarization state of the emitted light, polarization-resolved spectral measurements as in Fig. 2 play a crucial role. The polarization state of the eigenmodes is conveniently described with the orientation ϕ of the polarization ellipse and its ellipticity angle χ. This latter angle is given by $\chi=\arctan(E_y/E_x)$, where E_x and E_y are the field amplitudes along the long and the short ellipticity axis, respectively ($-45°\leq\chi\leq45°$). The polarization angle ϕ was measured by rotating a Glan-Thomson polarizer in front of the Fabry-Pérot interferometer such that the component under study was maximally suppressed in the spectrum; the ellipticity angle χ was determined in a similar way, but now by using the combination of a quarter-wave plate and the polarizer. For the lasing polarization, these angles could be determined with an accuracy of typically 0.3°, at least

when the polarization components could be spectrally resolved. Measurements on the nonlasing component were generally less accurate due to the proximity of the much stronger lasing polarization component for these measurements. The values for ϕ and χ were therefore measured for the lasing polarization component.

The first controlled anisotropy that we use is linear birefringence induced by means of the so-called hot-spot technique [18,19]. This technique consists of locally heating the surface of the array in the vicinity of the studied VCSEL by means of a tightly focused cw Ti-sapphire beam. The wavelength of this heating beam is tuned to a minimum in the reflection spectrum of the VCSEL (≈ 770 nm) to achieve sufficient absorption. Thermal expansion around the thus created hot spot induces strain and consequently birefringence in the VCSEL. The magnitude of the birefringence can be tuned in a continuous and reversible way by varying the applied heating power. This magnitude is found to be proportional to the temperature rise ΔT of the VCSEL that results from the heating with the hot spot; the temperature rise can be accurately deduced from the spectral shift of the lasing mode [18,19]. Also the orientation of the induced birefringence can be chosen at will by proper positioning of the hot spot on the surface of the array.

The second controlled anisotropy is circular birefringence induced by an axial magnetic field, i.e., a magnetic field parallel to the direction of beam propagation. For these experiments, the VCSEL array was positioned between the pole pieces of a strong electromagnet ($|B| \lesssim 0.5$ T). The VCSEL light was collimated with a lens mounted inside a center hole in one of the pole pieces; the experimental results were corrected for the (small) Faraday rotation in the collimating lens.

IV. CONSERVATIVE COUPLING

A. Strain-induced birefringence

In a linearly polarized basis set with its axes along [100] and [010], we find that the birefringence induced with the hot spot is described by [19]

$$\widetilde{M} = n^2 \omega_0 \gamma \Delta T \begin{pmatrix} \cos2\psi & A\,\sin2\psi \\ A\,\sin2\psi & -\cos2\psi \end{pmatrix}, \qquad (7)$$

where ψ denotes the orientation of the hot spot relative to [100]. The proportionality constant γ in this equation depends on the thermal expansion coefficient α [28], the elastic tensor components C_{ij} [28], and the elasto-optic tensor components p_{ij} [19] according to

$$\gamma = \frac{\alpha(C_{11}+2C_{12})(p_{11}-p_{12})}{24C_{11}}. \qquad (8)$$

The parameter A in Eq. (7) is the ratio of the anisotropy of the elasto-optic tensor and that of the elastic tensor, and expresses the anisotropy of the relation between stress and birefringence:

$$A = \frac{2p_{44}/(p_{11}-p_{12})}{2C_{44}/(C_{11}-C_{12})}. \qquad (9)$$

For an isotropic material, $A=1$, and inspection of Eq. (7) shows that in that case the axis of the birefringence is in the direction of the hot spot. In our VCSELs, the relation between stress and birefringence has been found to be anisotropic, with a measured value for the anisotropy factor $A=2.7$ [19]. In that case, the orientation ϕ of the induced birefringence is generally different from the orientation ψ of the hot spot. Note that also the magnitude of the induced birefringence depends on ψ.

For comparison with experiment, also the native birefringence in the VCSEL should be included in Eq. (7). For ease of notation we choose a basis set along the axes of the hot-spot induced birefringence, i.e., we diagonalize Eq. (7), and express the magnitude of the induced birefringence as $\delta_{\mathrm{hot}} \propto \Delta T$. If the native birefringence is oriented at an angle ϕ_0 with respect to the hot-spot induced birefringence, and if the native spectral splitting has a magnitude $\Delta\omega_0 = 2\delta_0$, the coupling matrix can be written as follows:

$$\widetilde{M} = \begin{pmatrix} (\delta_{\mathrm{hot}})' & \delta_0\,\sin2\phi_0 \\ \delta_0\,\sin2\phi_0 & -(\delta_{\mathrm{hot}})' \end{pmatrix}. \qquad (10)$$

In this expression, we have combined δ_{hot} with the x component of the native birefringence to $(\delta_{\mathrm{hot}})' = \delta_{\mathrm{hot}} + \delta_0 \cos2\phi_0$. Note that the coupling resulting from the native birefringence is maximum for $\sin2\phi_0 = \pm 1$ ($\phi_0 = \pm 45°$), in which case also $(\delta_{\mathrm{hot}})' = \delta_{\mathrm{hot}}$.

The eigenmodes of Eq. (10) are always linearly polarized, with an orientation ϕ given by

$$\tan2(\phi-45°) = \frac{(\delta_{\mathrm{hot}})'}{\delta_0\,\sin2\phi_0}. \qquad (11)$$

This expression shows that the orientation ϕ of the net birefringence rotates over 90° when $(\delta_{\mathrm{hot}})'$ is varied from $-\infty$ to ∞. Furthermore, the dependence of ϕ on $(\delta_{\mathrm{hot}})'$ is antisymmetric around $(\delta_{\mathrm{hot}})'=0$, i.e., around the situation for which $\phi=45°$. As a function of $(\delta_{\mathrm{hot}})'$, the frequency splitting $\Delta\omega$ shows the avoided crossing behavior of Fig. 1(a). By using Eq. (11), the frequency splitting can be written in a form that no longer explicitly depends on ΔT:

$$\Delta\omega = (\Delta\omega_0)_{\min}\sqrt{1+\tan^2 2(\phi-45°)}, \qquad (12)$$

where $(\Delta\omega_0)_{\min} = 2\delta_0 \sin2\phi_0$ is the frequency splitting for $(\delta_{\mathrm{hot}})'=0$, i.e., the minimum frequency splitting of the avoided crossing.

Figures 3 and 4 give an experimental demonstration of the behavior of ϕ and $\Delta\omega$, respectively, as a function of the hot-spot induced temperature rise ΔT of the VCSEL. For these measurements, the hot spot was oriented along the [010] direction ($\phi=90°$ in Fig. 3). For this particular position of the hot spot, the applied birefringence δ_{hot} will also be along the [010] axis [see Eq. (7)]. The native polarization of the lasing mode was oriented at an angle $\phi_0=21°$ from [100], i.e., at $-69°$ from the applied birefringence, and the lasing mode had the higher optical frequency. The solid curve in Fig. 3 is a fit through the data according to Eq. (11), i.e., to $\phi=45°+\frac{1}{2}\arctan[a(\Delta T - \Delta T_{\min})]$, using a and $\Delta T_{\min}$ as fitting parameters; note the excellent agreement with experiment. The next step is to analyze the mode-splitting results in Fig. 4. According to Eq. (12), these results should
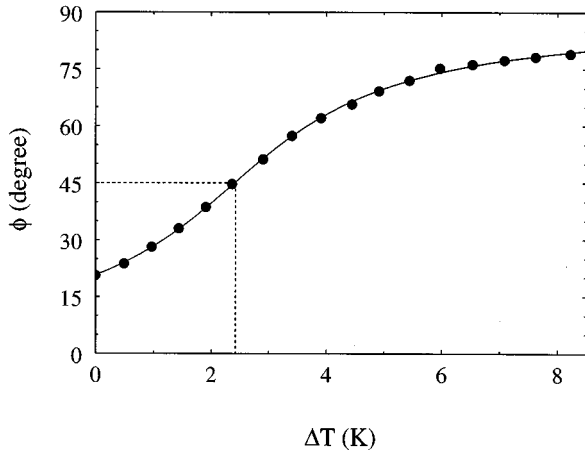
FIG. 3. Example of measured polarization orientation ϕ of the lasing mode, as a function of hot-spot-induced temperature rise ΔT in the VCSEL. The applied birefringence is in the [010] direction (90°), and is proportional to ΔT. The solid curve is a theoretical fit through the data. The dotted lines indicate the symmetry point of this fitted curve, i.e., $\phi=45°$ and $\Delta T=2.4$ K.

directly follow from the behavior of $\phi(\Delta T)$ already given in Fig. 3, in combination with $(\Delta\omega_0)_{\min}$, i.e., the minimum achieved spectral splitting at $\phi=45°$. We therefore used the measured value $(\Delta\omega_0)_{\min}$ and the relation for $\phi(\Delta T)$ to predict the data in Fig. 4. The dotted curve in this figure shows this predicted curve; although the overall behavior is very similar to the experimental results, a significant difference for the magnitude of the spectral splitting is found. This discrepancy is somewhat surprising, as the results for the polarization orientation as a function of ΔT were generally very accurately described with the linear model.

The discrepancy can be removed when we assume that the actual birefringence in the device is slightly smaller than
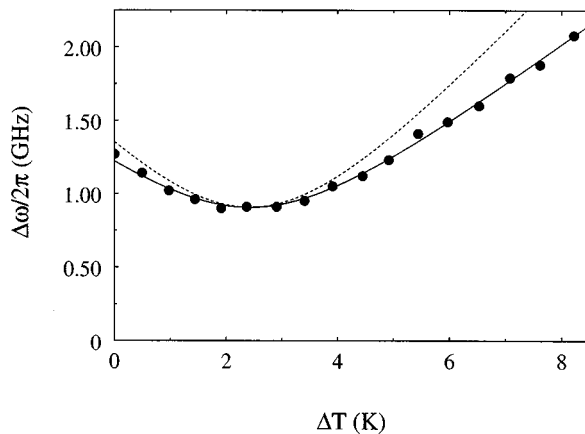

FIG. 4. Measured mode splitting $\Delta\omega/2\pi$ as a function of hot-spot-induced temperature rise ΔT in the VCSEL. The measurements correspond to those of Fig. 3. The dotted curve represents a theoretical prediction using the fitted relation between ϕ and ΔT from Fig. 3 and the measured mode splitting at the avoided crossing. The solid curve through the data has been derived from the dotted curve by assuming that the actual birefringence in the VCSEL is slightly smaller than expected from the measured frequency splitting (see text).
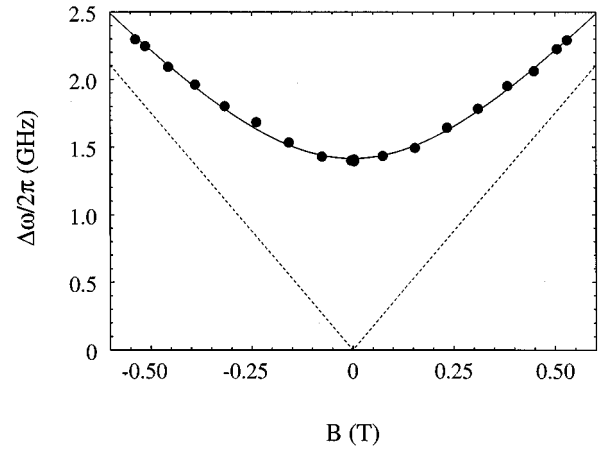

FIG. 5. Measured frequency splitting $\Delta\omega/2\pi$ as a function of magnetic-field strength B. The solid curve is a theoretical fit through the data; the dotted lines represent the calculated asymptotes of the frequency splitting.

expected from the measured mode splitting; we therefore decrease $(\Delta\omega_0)_{\min}$ in Eq. (12) by a small amount and add the same amount to the mode splitting as calculated on the basis of this reduced value of $(\Delta\omega_0)_{\min}$. The solid curve in Fig. 4 shows that excellent agreement can be obtained using a value for $(\Delta\omega_0)_{\min}$ that is only 0.2 GHz smaller than the actually measured minimum mode splitting. Also for other devices, measurements similar to those of Figs. 3 and 4 were excellently described by assuming that the measured mode splitting consisted of a part described with the linear model and a small offset. This deviation from the linear model cannot be explained by the presence of residual dichroism: using the method explained in Sec. V we explicitly checked that the birefringence was sufficiently large as compared to the dichroism that corrections to both the mode splitting and the polarization angle were negligible. Note, furthermore, that such dichroism will generally lead to a *decrease* instead of the observed *increase* of the mode splitting [cf. Fig. 1(b)]. The reason for the deviation might well be of a nonlinear nature and could thus signal a limit to the validity of approximating Eq. (1) with the linear model.

B. Application of an axial magnetic field

As a second demonstration of conservative coupling, we consider the influence of an axial magnetic field B on the polarization properties. The magnetic field leads to a Faraday effect in the semiconductor materials of both the active layer and the Bragg mirrors, i.e., it leads to a different refractive index for left- and right-handed circularly polarized light [$n(\sigma^+)\neq n(\sigma^-)$]. As experimentally demonstrated in Ref. [20], the magnetic field changes the polarization of a VCSEL from linear to elliptical; if B is reversed the ellipticity changes sign. The ellipticity shows a gradual increase as a function of the magnetic field, and is accompanied by a change of the mode spectrum. An example of the measured frequency splitting as a function of the magnetic field is shown in Fig. 5. Note again the clear avoided crossing behavior.

Generally, an excellent fit to the experimental results was obtained by regarding the combined effect of circular and

linear birefringence. For that, we express the coupling matrix in a circularly polarized basis, which leads to the following expression for the evolution of the optical field:

$$\frac{\partial}{\partial t}\begin{pmatrix} E_+ \\ E_- \end{pmatrix} = i\begin{pmatrix} \Omega & \delta_0 \\ \delta_0 & -\Omega \end{pmatrix}\begin{pmatrix} E_+ \\ E_- \end{pmatrix}. \qquad (13)$$

The Faraday effect enters as a detuning of the circularly polarized basis states ($\Omega \propto B$), whereas the native birefringence enters as the coupling δ_0 between these basis states. The frequency difference between the (elliptically) polarized eigenmodes is found in a straightforward way:

$$\Delta\omega = \Delta\omega_0\sqrt{1+(\Omega/\delta_0)^2}, \qquad (14)$$

where $\Delta\omega_0 = 2\delta_0$ is the native birefringence splitting, i.e., for $\Omega = 0$ ($B=0$). Experimentally, B is known; therefore the strength of the Faraday effect, i.e., $d\Omega/dB$, is the only unknown parameter in this equation. Fitting Eq. (14) through the data in Fig. 5 yielded the value $(d\Omega/dB)/2\pi = 1.7$ GHz T^{-1}. The solid curve in Fig. 5 shows the fitted curve; note the excellent agreement with the experiment. The dotted lines in the figure represent the asymptotes of the mode splitting (i.e., for $B \to \pm\infty$) based on the fitted value of $d\Omega/dB$.

Measurements on devices with very small birefringence, i.e., for $|\Delta\omega_0/2\pi| < 1$ GHz, could sometimes not be properly described with Eq. (13), i.e., by considering only circular and linear birefringence. For instance, sometimes a rotation of the ellipticity axis was observed upon increasing the magnetic field. Furthermore, on some occasions such measurements revealed that the ellipticity axis of the lasing polarization component was not perpendicular to that of the nonlasing component, but deviated by a small amount $\Delta\phi \lesssim 3°$. These observations cannot be understood by considering only birefringence: the axes of the elliptical polarization eigenmodes of Eq. (13) coincide with the axes of the birefringence, i.e., they remain fixed and are mutually perpendicular, irrespective of the value of $\Omega(B)$. That this is not always the case for small birefringence does not necessarily indicate that the linear model breaks down: in practice also a small amount of dichroism is present (see Sec. V), which requires addition of extra (anti-Hermitian) terms in Eq. (13). Note that inclusion of linear dichroism in Eq. (13) will make the description of the polarization state as a function of B substantially more complicated, as two more parameters (i.e., the orientation and magnitude of the dichroism) will be needed to describe $\widetilde{M}$. We have not yet pursued this in a quantitative manner, but in principle dichroism can explain the experimental observation that the (relative) orientation of the polarization ellipse varies as a function of the magnetic field.

V. MIXED COUPLING

Experimentally, careful analysis of the polarization state of our VCSELs reveals that the lasing mode has generally a small residual ellipticity ($|\chi| < 4°$) even in the absence of a magnetic field. The presence of this residual ellipticity can, for instance, be inferred from Fig. 2: in this figure, the lasing component cannot be completely blocked with the polarizer, but a small fraction ($\approx 10^{-4}$) remains visible in the spectrum. With the combination of a quarter-wave plate and the polar-

izer, however, suppression of the lasing component to better than 10^{-6} can be achieved, the suppression now being limited by the quality of the polarizer. This demonstrates that lasing occurs in a pure mode which, however, is not completely linearly polarized, but has a small residual ellipticity. Within the linear mode-coupling framework, this ellipticity for zero magnetic field can only be explained by the simultaneous presence of linear birefringence and linear dichroism, their orientations being different. For the results presented in Sec. IV A and in previous articles [18–20], this dichroism could be neglected from the analysis, as in these experiments the birefringence largely dominates the polarization state. As will be demonstrated in Sec. V B, the effect of dichroism can be rather dramatic if the hot-spot technique is used to achieve complete cancellation of the native birefringence. To understand these measurements, it is necessary to know *a priori* the magnitude and orientation of the residual dichroism; we will therefore first concentrate on how these can be determined with the hot-spot technique.

When birefringence and dichroism are both present, the coupling matrix can be written in the following form:

$$\widetilde{M} = \begin{pmatrix} \delta + i\gamma\cos2\Delta\phi & i\gamma\sin2\Delta\phi \\ i\gamma\sin2\Delta\phi & -(\delta + i\gamma\cos2\Delta\phi) \end{pmatrix}, \qquad (15)$$

where we have chosen a linearly polarized basis set with its axes along those of the net birefringence δ, i.e., the sum of the native and hot-spot induced birefringence. The dichroism is characterized with its magnitude γ, and with its orientation $\Delta\phi$ with respect to the birefringence.

Contrary to the situations described in Sec. IV, the eigenmodes of Eq. (15) are generally not orthogonal. It is straightforward to show that the polarization eigenmodes have in fact equal ellipticity and equal helicity, in contrast to equal ellipticity and opposite helicity as in the case of Hermitian $\widetilde{M}$. Furthermore, the major axes of the polarization ellipses of the two eigenmodes are always perpendicular. These statements only hold in the absence of a magnetic field: inclusion of circular birefringence in Eq. (15) will generally result in elliptical eigenpolarizations with mutually nonperpendicular orientations and with different ellipticities (cf. the situation described in the last paragraph of Sec. IV B).

Equation (15) reduces to the form of Eq. (4), i.e., the coupling becomes purely dissipative, for $\Delta\phi = \pm45°$. As a function of δ the eigenfrequencies then behave as in Fig. 1(b). For $|\delta| > |\gamma|$, the ellipticity axes are oriented along those of the birefringence ($\phi = 0°$ and $90°$) and the ellipticity of both eigenmodes is given by

$$\tan2\chi = \gamma/\sqrt{\delta^2 - \gamma^2}. \qquad (16)$$

For $|\delta| < |\gamma|$, i.e., in the frequency locking region, the ellipticity axes are oriented along those of the dichroism ($\phi = \pm45°$), and the ellipticity is given by

$$\tan2\chi = \delta/\sqrt{\gamma^2 - \delta^2}. \qquad (17)$$

Note that except for $\delta = 0$, the eigenmodes are always elliptically polarized, whereas for the particular situation that $|\delta| = |\gamma|$ the eigenmodes are circularly polarized ($\chi = \pm45°$), i.e., the ellipticity achieves its maximum value. Note, further-

more, that in this latter situation both the real and the imaginary parts of the eigenfrequencies are degenerate.

The coupling introduced by the dichroism is maximum for the just described dissipative coupling case ($\Delta\phi=\pm45°$). In contrast, no coupling is present when the axes of the birefringence and those of the dichroism are aligned ($\Delta\phi =0°$); in that case the eigenmodes are always linearly polarized. General expressions for $\Delta\omega$, χ, and ϕ for arbitrary orientation $\Delta\phi$ of the dichroism can be derived in a straightforward way, but are substantially more complicated than for the situations mentioned above. For fixed values of δ and γ, all parameters vary in a continuous way between those found for the maximally coupled and the uncoupled situation. Generally, the mode splitting will be smaller than without the dichroic coupling, the eigenmodes will be elliptically polarized, and the orientation ϕ of the polarization ellipse will coincide neither with the orientation of the birefringence nor with the orientation of the dichroism.

For the situation in which the dichroism is much smaller than the birefringence, i.e., $|\gamma|\ll|\delta|$, simple approximate expressions can be found that are useful for the determination of the orientation and magnitude of the dichroism. To first order, both the orientation of the polarization ellipse and the spectral splitting have the same values as without dichroism. The ellipticity, however, does depend to first order on γ/δ:

$$\chi\approx\frac{\gamma}{2\delta}\sin2\Delta\phi. \tag{18}$$

Note that this expression is exact for the uncoupled situation ($\Delta\phi=0$). The difference in damping of the (elliptically polarized) eigenmodes is, to first order, given by

$$\Delta\gamma\approx\Delta\gamma_0\cos2\Delta\phi, \tag{19}$$

where we have introduced $\Delta\gamma_0=2\gamma$ for the magnitude of the dichroism. This expression is exact both for $\Delta\phi=\pm45°$ and $0°$; in the first situation the two (elliptically polarized) eigenmodes have equal damping, whereas in the latter situation the difference in damping of the (linearly polarized) eigenmodes is determined only by the dichroism.

A. Experimental determination of residual dichroism

Equation (18) suggests that both the magnitude and the orientation of the dichroism can be determined by varying the orientation of the birefringence. Figure 6 shows the results of such measurements for two different devices, both operated at $1.3I_{\mathrm{thr}}$. The hot-spot technique was used to rotate the polarization (cf. Sec. IV A) in such a way that for each individual measurement the resulting mode splitting was equal to its native value $\Delta\omega_0$. The orientation ϕ of the polarization (or, to first order, of the net birefringence) in this figure is expressed relative to the [100] crystalline axis. The two devices used have different values of the native birefringence: $\Delta\omega_0/2\pi=1.4$ GHz for the solid dots and $\Delta\omega_0/2\pi=-1.2$ GHz for the open dots, where a positive value for $\Delta\omega$ indicates that the lasing mode has the higher optical frequency. For both devices, the native polarization orientation ϕ_0 was about 40°.

As expected, the measured ellipticity varies as a function of the orientation ϕ of the birefringence. The two dashed
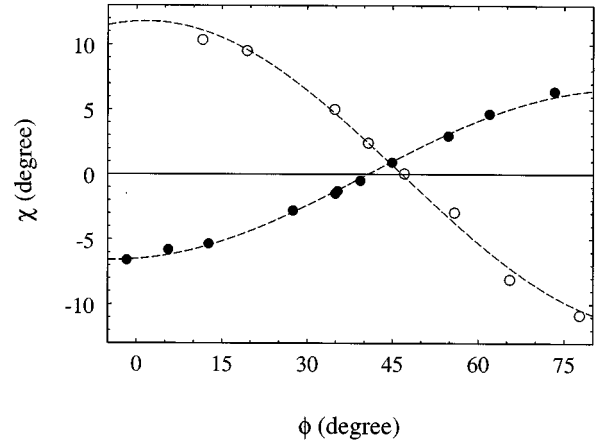

FIG. 6. Ellipticity angle χ as a function of polarization orientation ϕ relative to [100]. The two data series correspond to different lasers with opposite sign of the native birefringence (see text). The dashed curves are theoretical fits through the data.

curves are fits through the data according to Eq. (18), i.e., to $\chi=\chi_0\sin[2(\phi-\phi_\gamma)]$, with the orientation ϕ_γ of the dichroism and the amplitude χ_0 as fitting parameters. The positions of the zero crossings of these curves, i.e., the angles where the light is exactly linearly polarized, directly yield the orientations ϕ_γ of the dichroism. For the measurements represented by the solid and open data points we find $\phi_\gamma=41°$ and 47°, respectively. The fitted parameter χ_0 in combination with the value of the native birefringence splitting $\Delta\omega_0=2\delta$ yields the magnitude $\Delta\gamma_0$ of the dichroism. Note that χ_0 is of opposite sign for the two data series; as the native spectral splitting is also of opposite sign for the two measurements series, this indicates that the sign of the dichroism is equal for the two devices. From the fitted curves, we find $\Delta\gamma_0/2\pi=-0.32$ and -0.49 GHz for the data represented with the solid and the open dots, respectively. This leads to $|\gamma/\delta|\approx0.3$, so that we satisfy the first-order approximation implied in Eqs. (18) and (19). The thus determined sign and orientation of the dichroism indicates that, as to be expected, the lasing polarization component has the lower loss for all measurements in the $\approx90°$ interval of polarization angles plotted in Fig. 6. Furthermore, when the polarization is rotated more than 45° away from ϕ_γ, it was found that lasing had switched to the orthogonal polarization component, which, according to Eq. (19) then has the lowest loss. These findings leave little room for a role of nonlinear anisotropies in selecting the lasing polarization.

Also the spectral width of the nonlasing mode was observed to vary as a function of ϕ. This behavior is illustrated in Fig. 7, where the measured full widths at half maximum (FWHM) widths, corrected for the instrumental resolution of the Fabry-Pérot interferometer, are shown as a function of the orientation ϕ of the birefringence. The measurements correspond to those of the solid dots in Fig. 6. The width is largest around $\phi=\phi_\gamma=41°$ [$\Delta\phi=0°$ in Eq. (19)], and shows a gradual decrease when $\Delta\phi$ changes towards $\pm45°$. We expect that these measured widths are directly related to the imaginary part Γ of the eigenvalue of the nonlasing, i.e., the spontaneous emission mode ($\Delta\omega_{\mathrm{FWHM}}=2\Gamma$). We do not know the *total* loss rate Γ for the spontaneous emission
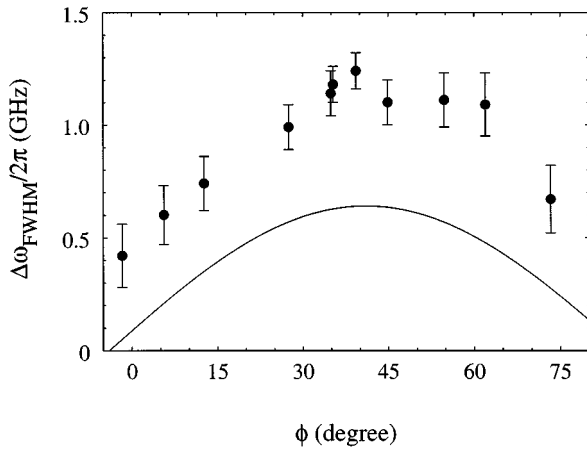
FIG. 7. Measured width of nonlasing polarization component as a function of the polarization orientation ϕ of the lasing component. The data correspond to the measurements of the solid dots in Fig. 6. The solid curve represents the theoretical behavior of the difference between the widths of the two cavity resonances, using the determined values of the dichroism of Fig. 6 (see text).

FIG. 8. Example of measured ellipticity angle χ as a function of injection current I. The dashed curve shows the calculated ellipticity, based on an independent experimental determination of the birefringence and the dichroism.

mode, but we *do* know the difference of its loss rate with that of the lasing mode, namely, $\Delta\gamma(\phi)$ as found from Fig. 6 and Eq. (19). For comparison with experiment, we plotted $|2\Delta\gamma(\phi)|$ as the solid curve in Fig. 7. Although the measured widths are appreciably above this calculated curve, the behavior as a function of ϕ is rather similar. Part of the discrepancy is certainly due to the finite width of the lasing component (≈ 0.2 GHz), which produces an offset of the solid curve. The rest of the discrepancy remains unexplained and might have the same origin as the offset found earlier in Fig. 4.

The dichroism was measured for various devices and at different values of the injection current. Generally, the magnitude of the dichroism showed a gradual decrease with increasing current. Its orientation also showed a gradual change with current, but the magnitude and direction of this change were different from VCSEL to VCSEL. For various devices and at various values of the injection current, we measured values for $\Delta\gamma_0/2\pi$ between 0.1 and 1.0 GHz. The orientation of the dichroism was found to be always within $20°$ from the [110] crystalline direction.

The measurements described above indicate that knowledge of both the native birefringence and of the native dichroism is essential for a proper description of the polarization state of VCSELs. To demonstrate this further, we measured the polarization state of a specific device as a function of the injection current; Fig. 8 shows the measured ellipticity. For this device the threshold current was 5.5 mA, whereas first-order transverse modes appeared as late as $I\approx 10$ mA. The measurements show a pronounced change of the ellipticity angle χ with current; the ellipticity even reverses sign around $I=9$ mA. The orientation ϕ of the polarization ellipse also showed a gradual change with injection current which, however, amounted to only $2.1°$ in the range depicted in the figure. The measured mode splitting showed a gradual decrease with current from $\Delta\omega/2\pi=1.80$ GHz at $I=6$ mA to $\Delta\omega/2\pi=1.05$ GHz at $I=10$ mA. Based on inspection of the birefringence alone, one would have expected
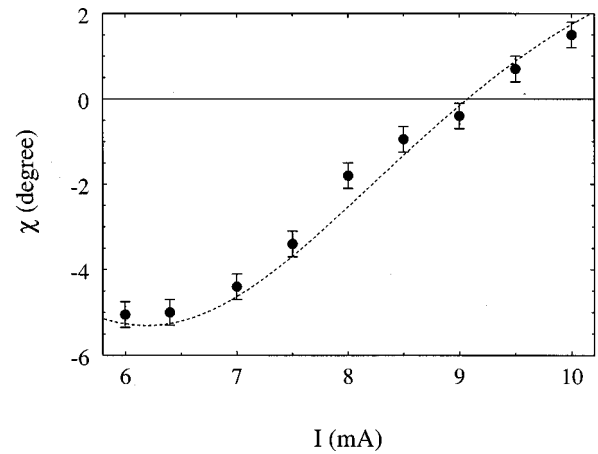
an *increase* instead of the observed decrease of the ellipticity with injection current. These measurements are an interesting test case for the linear model: as rather high injection currents are involved, one could wonder whether the decrease with injection current should be ascribed to nonlinear effects. In order to see whether the linear model holds throughout the current range depicted in Fig. 8, the current dependence of all four independent parameters has to be measured. Determination of the magnitude and orientation of the birefringence as a function of the injection current is done in a straightforward way by measuring the birefringence splitting $\Delta\omega$ and the polarization orientation ϕ. Determination of the magnitude and orientation of the dichroism is done using measurements as in Fig. 6, which requires considerably more work. The dichroism was measured at 6, 7, 8, and 9 mA. Its magnitude was found to decrease from $\Delta\gamma_0/2\pi=-0.68$ GHz at $I=6$ mA to -0.38 GHz at $I=9$ mA. The orientation ϕ_γ of the dichroism, and therefore also the angle $\Delta\phi$ between dichroism and birefringence, showed a pronounced change with current. At $I=6$ mA, $\Delta\phi$ was as large as $15°$, whereas the birefringence and dichroism were roughly aligned (i.e., $\Delta\phi=0°$) at $I=9$ mA. After having determined both the birefringence and the dichroism as a function of the injection current, we can use Eq. (18) to predict the ellipticity as a function of the injection current. This yields the dotted curve in Fig. 8, which shows very good agreement with experiment. It should be noted that no free parameters were involved to obtain this curve. The observed change of the ellipticity with current is found to be dominated by the changes in $\Delta\omega$ and $\Delta\phi$: the decrease of the birefringence tends to increase the ellipticity, which, however, is counteracted by the rotation of the dichroism in the direction of the birefringence. The example shown in Fig. 8 also demonstrates that it is difficult to formulate general statements on the behavior of the polarization state as a function of the injection current: generally, all four parameters needed for the linear model show seemingly uncorrelated variations with injection current.

B. Polarization behavior of nearly isotropic VCSELs

The hot-spot technique can also be used to completely cancel the native birefringence in a VCSEL. For that pur-
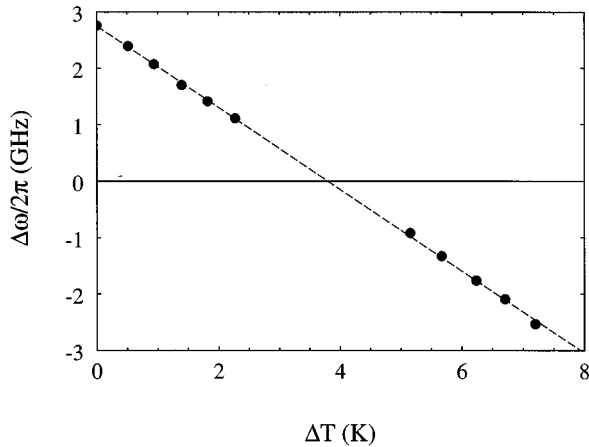
FIG. 9. Measured spectral splitting $\Delta\omega/2\pi$ as a function of hot-spot induced temperature rise ΔT. Due to the intrinsic widths of the spectral components, the mode splitting could not be resolved in the range $\Delta T\approx2.5$–5.0 K. The dashed line is a linear regression through the data, which has its zero crossing at $\Delta T=3.8$ K.

pose, the applied birefringence should be exactly in the same direction and of opposite sign. An example of such measurements is shown in Figs. 9 and 10. The solid dots in Fig. 9 show the measured frequency difference $\Delta\omega$ between the lasing and nonlasing polarization component as a function of the hot-spot induced temperature rise ΔT. The solid line in this curve is a linear regression through the data, which suggests a frequency crossing at $\Delta T=3.8$ K. Note that there are no data points near the actual zero crossing; the reason is that the individual polarization components cannot be spectrally resolved near the crossing due to their intrinsic widths (≈0.8 GHz for the spontaneous emission mode). In this region, however, measurement of the polarization state is still possible because the lasing component is much stronger than the spontaneous emission mode. Figure 10 shows the measured polarization angles and ellipticity angles as a function of ΔT. The native polarization orientation was at 44.5° from [100];
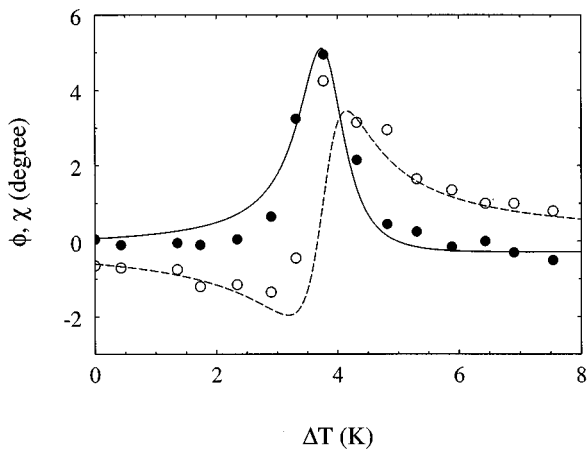

FIG. 10. Polarization angle ϕ (solid dots) and ellipticity angle χ (open dots) as a function of hot-spot induced temperature rise ΔT. The data correspond to the measurements in Fig. 9. The curves through the data represent theoretical fits based on an independent determination of the dichroism.
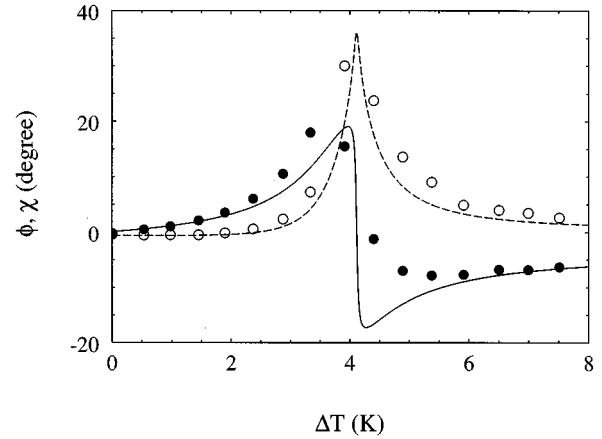

FIG. 11. Polarization angle ϕ (solid dots) and ellipticity angle χ (open dots) as a function of hot-spot induced temperature rise ΔT. The measurements were performed on the same device as in Figs. 9 and 10, but with a slightly different orientation of the controlled birefringence. The minimum net birefringence occurs at $\Delta T=4.0$ K, as found from the accompanying measurements of the spectral splitting. The curves through the data represent the theoretical fits (see text).

for ease of presentation we have denoted this native orientation as $\phi=0°$. Near the crossing at $\Delta T=3.8$ K, the polarization rotates slightly (solid dots), whereas we also observe a small variation of the ellipticity with ΔT (open dots).

To explain this behavior, both the orientation and magnitude of the dichroism were determined in a separate experiment as described in Sec. V A. The dichroism was found to be oriented at $\varphi_\gamma=+5°\pm1°$, which agrees with the polarization orientation observed at $\Delta T=3.8$ K in Fig. 10. This suggests that the dichroism is responsible for the behavior of the polarization state as a function of ΔT in Fig. 10. As a further check, we used the measured values of the dichroism to predict the ellipticity as a function of ΔT. In fact, the best agreement between the experimental and the calculated behavior was achieved by assuming a small misalignment $\Delta\varphi=-0.2°$ between the native and applied birefringence; the calculated polarization and the ellipticity angles are shown by the solid and the dotted curve in Fig. 10, respectively.

The behavior of the polarization state around the anticipated zero crossing shows a dramatic change if the angle $\Delta\varphi$ between the applied and the native birefringence is only slightly increased with respect to the measurements of Figs. 9 and 10. An example thereof is shown in Fig. 11; this measurement was performed on the same device and at the same injection current as the preceding experiment. Note the difference of the vertical scale as compared to that of Fig. 10. The misalignment $\Delta\varphi$ of the orientation of the applied birefringence can be inferred from the "asymptotic" value of the polarization angle, namely, $\Delta\varphi=3.2°$. Again, the solid and the dotted curve are calculated curves for the polarization angle and the ellipticity (see below).

Comparison of Figs. 10 and 11 shows that the behavior around the anticipated zero crossing is very sensitive to a misalignment of the orientation of the native and the applied birefringence. This can be understood by first considering the effect of this misalignment on the (net) birefringence as a function of ΔT: this will lead to the avoided crossing behav-

ior of the (net) birefringence as described in Sec. IV A. Also the orientation of the birefringence will vary as a function of ΔT, the change being most prominent around the avoided crossing. For the results in Fig. 10, the misalignment $\Delta \varphi$ between the native and the applied birefringence was small ($\approx 0.2°$), and the minimum achieved birefringence is estimated as $(\Delta \omega / 2\pi)_{min} = 0.02$ GHz (cf. Sec. IV A). This is much smaller than the experimentally determined magnitude of the dichroism $\Delta \gamma_0 / 2\pi = -0.30 \pm 0.05$ GHz. The dichroism will thus dominate the polarization properties near the anticipated zero crossing for the mode splitting in Fig. 9. For the results in Fig. 11, however, the misalignment $\Delta \varphi$ is an order of magnitude larger, so that the minimum magnitude of the birefringence is comparable to that of the dichroism. The polarization state will therefore be much more sensitive to the variation of the relative orientation of the dichroism and birefringence that occurs around the anticipated zero crossing of the mode splitting. This explains the large variations of both the polarization angle and the ellipticity in Fig. 11. Furthermore, the theoretically calculated behavior of the polarization state was found to depend strongly on the precise magnitude of the dichroism, which is again consistent with the fact that for these measurements the minimum birefringence is comparable to the magnitude of the dichroism. The calculated behavior of the polarization state was found to fit best to the experimental data when using $\Delta \gamma_0 / 2\pi = -0.33$ GHz, which nicely corresponds to the other measurement of this quantity.

The theoretical curves in Figs. 10 and 11 were calculated using the same values of the dichroism ($\varphi_\gamma = 5°$ and $\Delta \gamma_0 / 2\pi = -0.33 \pm 0.05$ GHz). The misalignment angle $\Delta \varphi$ was thus the only free parameter in these calculations ($\Delta \varphi = -0.2°$ for Fig. 10 and $\Delta \varphi = -3.2°$ for Fig. 11). The calculated behavior agrees reasonably with that found from experiment. In this context, it should be noted that the accuracy of the measurements is limited around the position of the zero crossing for $\Delta \nu$. This is mainly due to the large variations of ϕ and χ as a function of ΔT in this region: accurate determination requires extreme stability of the magnitude of the applied birefringence (or, equivalently, of the power of the Ti-sapphire heating beam). Furthermore, the fact that the two polarization components cannot be spectrally resolved, also somewhat decreases the accuracy.

VI. CONCLUDING DISCUSSION

By applying a controllable amount of either linear or circular birefringence to our VCSELs, we have examined the influence of these anisotropies on their polarization state. The results were found to be in good agreement with a linear rate-equation model that describes the influence of linear anisotropies on the vectorial cavity eigenmodes. The analysis shows that the polarization state is generally determined by the combined effect of different anisotropies. As an example thereof, we experimentally demonstrated and quantified the presence of residual dichroism. This dichroism was shown to explain the observation that the emitted light is generally elliptically polarized even in the absence of a magnetic field.

The origin of the dichroism is not clear at present. It could be related to growth on a (slightly) misoriented substrate. Such tilting, typically a few degrees, provides a feasible ex-

planation for our observation that for all lasers the dichroism is roughly along one specific orientation, corresponding to a face-diagonal crystalline axis ([110] or [1$\bar{1}$0]). It cannot, however, explain the observed spread of both the magnitude and orientation of the dichroism. Note that the measured dichroism is not necessarily the only mechanism that leads to a difference in loss for two polarization eigenmodes: when the modes have a different frequency, they will naturally experience a difference in loss due to the spectral dependence of the gain. However, this mechanism cannot change the polarization state of the cavity eigenmodes, and the experimental determination of the dichroism as described in this section is in fact insensitive to the spectral dependence of the gain. The spectral splitting of the cavity modes will only give rise to an extra contribution to their loss; note that in fact this will codetermine the selection of one of the two polarization modes.

The linear description suggests a convenient way to study the effect of such a loss difference in a VCSEL in a systematic way. The loss difference that results from the dichroism can be varied in a continuous way between $\pm \Delta \gamma_0$ by changing the orientation of the birefringence. The net loss difference, i.e., the sum of that resulting from the dichroism and that of the spectral dependence of the gain, will depend on the magnitude of the spectral splitting and on the orientation between birefringence and dichroism. The net loss difference can thus be changed at will by varying both the magnitude and the orientation of the birefringence. Specifically the polarization behavior of devices which have been prepared such that the eigenmodes have equal loss is an interesting subject for future research.

The ellipticity resulting from the simultaneous presence of both birefringence and dichroism is most evident for situations in which the native birefringence was nearly canceled. In fact, we showed that nearly circularly polarized emission can result when the magnitude of the linear birefringence is roughly equal to that of the residual dichroism. This is a demonstration of the fact that the polarization state is determined by the *ratio* of the various anisotropies, rather than by their absolute values. This observation can be of importance for the development of methods to stabilize the polarization of VCSELs: from a fabrication point of view it might be simpler to decrease a particular anisotropy than to increase another one.

Our experimental results were generally in good agreement with the coupled-mode model. We found, however, also a few discrepancies between the experiments and the predictions of the linear model. The first discrepancy was found in Sec. IV A, where we measured the behavior of both the polarization angle and the mode splitting as a function of the applied birefringence. Combination of these measurements revealed that the spectral splitting was slightly larger (≈ 0.2 GHz) than expected from the linear model. Also the spectral width of the nonlasing mode was found to be larger than expected from a simple linear argument based on the measured dichroism (Sec. V A). It is interesting to note that we found a similar offset in another context, namely, for devices that showed a switch to the other polarization mode upon increasing the injection current. In these situations, the mode splitting before and after the switch was different by an amount ranging from 0.3 to 1 GHz. The results indicate that

the frequency of the lasing polarization component is slightly higher than expected from the linear model, which is consistent with the measurements presented in Sec. IV A. To explain these discrepancies, it will be necessary to consider also the nonlinear terms in Eq. (1). We stress, however, that discrepancies were only observed for the spectrum of the emitted light; the polarization orientation and ellipticity were still in good agreement with the linear model. Even for the smallest achieved linear anisotropy in the present experiments, which was limited to about 0.3 GHz by the presence of residual dichroism, the polarization state could still be accurately described by considering only the measured linear anisotropies. Apparently, under the present experimental conditions, i.e., for linear anisotropies $\gtrsim 0.5$ GHz, nonlinear effects do not influence the polarization state.

This conclusion may be compared with a recent theoretical discussion of the polarization behavior of VCSELs which includes nonlinear effects [24,29,30]. In that work the quantum well gain medium of the VCSEL is modeled, in the spirit of gas-laser theory, as an atomic four-level scheme, introducing populations of spin $+\frac{1}{2}$ and $-\frac{1}{2}$ electrons and spin $+\frac{3}{2}$ and $-\frac{3}{2}$ (heavy) holes. Apparently the competition between the σ^+ and σ^- modes that couple to the $\pm\frac{1}{2}\leftrightarrow\pm\frac{3}{2}$ transitions is sufficiently close to neutral that in practical VCSELs the preference for linear polarization is imposed by the dominant linear anisotropy (namely, the birefringence). Nonlinear effects could still play an important role in switching between the two linear orthogonal polarizations of a VCSEL [30].

It would be interesting to investigate the polarization properties for even smaller linear anisotropies than achieved so far. For this purpose, control of also the linear dichroism is required. This could, for instance, be achieved by applying (weak) polarization-anisotropic feedback, as has been demonstrated for gas lasers [31]. When all linear anisotropies are sufficiently reduced, one expects that nonlinear anisotropy of the gain, i.e., anisotropy of the gain saturation, will start to dominate the polarization properties. Note, however, that in the present experiments the minimum achieved magnitude of the linear anisotropies is already comparable to the spectral widths of the individual polarization components. These widths are a measure for the quantum noise in the devices: eventually the polarization will start to diffuse under the influence of spontaneous emission. The region on the Poincaré sphere over which this diffusion takes place will strongly depend on the precise form of the nonlinear anisotropy of the gain [32].

In conclusion, we have demonstrated that the polarization of a VCSEL is dominantly determined by linear optical anisotropies. The relative importance of the various anisotropies was addressed in a quantitative way. So far, nonlinear effects were found to influence the polarization eigenmodes only to a minor extent. To achieve a fundamental understanding of also the nonlinear effects, aiming for a perfectly isotropic VCSEL forms a natural learning route.

[1] T. Ohtoshi, T. Kuroda, A. Niwa, and S. Tsuji, Appl. Phys. Lett. **65**, 1886 (1994).

[2] T. Numai, K. Kurihara, K. Kühn, H. Kosaka, I. Ogura, M. Kajita, H. Saito, and K. Kasahara, IEEE J. Quantum Electron. **31**, 636 (1995).

[3] Y. Kaneko, S. Nakagawa, T. Takeuchi, D. E. Mars, N. Yamada, and N. Mikoshiba, Electron. Lett. **31**, 805 (1995).

[4] C. J. Chang-Hasnain, J. P. Harbison, G. Hasnain, A. von Lehmen, L. T. Florez, and N. G. Stoffel, Electron. Lett. **27**, 163 (1991).

[5] C. J. Chang-Hasnain, J. P. Harbison, G. Hasnain, A. C. von Lehmen, L. T. Florez, and N. G. Stoffel, IEEE J. Quantum Electron. **27**, 1402 (1991).

[6] K. D. Choquette, D. A. Richie, and R. E. Leibenguth, Appl. Phys. Lett. **64**, 2062 (1994).

[7] K. D. Choquette, R. P. Schneider, K. L. Lear, and R. E. Leibenguth, IEEE J. Sel. Topics Quantum Electron. **1**, 661 (1995).

[8] Y. H. Chen, C. I. Wilkinson, J. Woodhead, C. C. Button, J. P. R. David, M. A. Pate, and P. N. Robson, Electron. Lett. **32**, 559 (1996).

[9] S. Jiang, Z. Pan, M. Dagenais, R. A. Morgan, and K. Kojima, Appl. Phys. Lett. **63**, 3545 (1993).

[10] H. Kawaguchi, I. S. Hidayat, Y. Takahashi, and Y. Yamayoshi, Electron. Lett. **31**, 109 (1995).

[11] A. K. Jansen van Doorn, M. P. van Exter, and J. P. Woerdman, Electron. Lett. **30**, 1941 (1994).

[12] A. Chavez-Pirson, H. Ando, H. Saito, and H. Kanbe, Appl. Phys. Lett. **62**, 3082 (1993).

[13] T. Mukaihara, F. Koyama, and K. Iga, Photon. Technol. Lett. **5**, 133 (1993).

[14] T. Yoshikawa, H. Kosaka, K. Kurihara, M. Kajita, Y. Sugimoto, and K. Kasahara, Appl. Phys. Lett. **66**, 908 (1995).

[15] K. D. Choquette and R. E. Leibenguth, Photon. Technol. Lett. **6**, 40 (1994).

[16] J.-H. Ser, Y.-G. Ju, J.-H. Shin, and Y. H. Lee, Appl. Phys. Lett. **66**, 2769 (1995).

[17] K. D. Choquette, K. L. Lear, R. E. Leibenguth, and M. T. Asom, Appl. Phys. Lett. **64**, 2767 (1994).

[18] A. K. Jansen van Doorn, M. P. van Exter, and J. P. Woerdman, Appl. Phys. Lett. **69**, 1041 (1996).

[19] A. K. Jansen van Doorn, M. P. van Exter, and J. P. Woerdman (unpublished).

[20] A. K. Jansen van Doorn, M. P. van Exter, M. Travagnin, and J. P. Woerdman, Opt. Commun. **133**, 252 (1997).

[21] W. van Haeringen, Phys. Rev. **158**, 256 (1967).

[22] H. de Lang, D. Polder, and W. van Haeringen, Philips Tech. Rev. **32**, 190 (1971).

[23] D. Lenstra, Phys. Rep. **59**, 299 (1980).

[24] M. Travagnin, M. P. van Exter, A. K. Jansen van Doorn, and J. P. Woerdman, Phys. Rev. A **54**, 1647 (1996).

[25] J. P. Woerdman and R. J. C. Spreeuw, *Analogies in Optics and Micro Electronics*, edited by D. Lenstra and W. van Haeringen (Kluwer, Dordrecht, 1990), p. 135.

[26] Vixel Corporation, 325 Interlocken Parkway, Broomfield, CO 80021, U.S.A.; Model No. PRI-LA-S-850-1×16-3S, Serial Nos. 2765 and 2767.

[27] A. K. Jansen van Doorn, M. P. van Exter, and J. P. Woerdman (unpublished).

[28] S. Adachi, J. Appl. Phys. **58**, R1 (1985).

[29] M. San Miguel, Q. Feng, and J. V. Moloney, Phys. Rev. A **52**, 1728 (1995).

[30] J. Martín-Regalado, M. San Miguel, N. B. Abraham, and F. Prati, Opt. Lett. **21**, 351 (1995).

[31] H. de Lang, Philips Res. Rep. Suppl. **8**, 1 (1967).

[32] M. A. van Eijkelenborg, C. A. Schrama, and J. P. Woerdman, Opt. Commun. **119**, 97 (1995).